

Electron-Electron Scattering as a Probe of Anomalous Gauge Couplings

Debajyoti Choudhury and Frank Cuypers

*Max-Planck-Institut für Physik, Werner-Heisenberg-Institut,
D-80805 München, Germany*

Emails: debchou, cuypers@iws166.mppmu.mpg.de

Abstract

The effect of anomalous gauge couplings on polarized e^-e^- scattering cross sections is examined. It turns out that different combinations of beam polarizations provide constraints that are complementary to each other and to those obtained from other experiments, such as e^+e^- , $e^-\gamma$ and $\gamma\gamma$ collisions.

1 Introduction

In general, electron colliders are implicitly assumed to be electron-positron colliders. At one of the projected linear colliders such as CLIC, JLC, TESLA, VLEPP, *etc.*, this need not necessarily be the case. Indeed, one or both electron beams could in principle be converted into a high energy real photon beam by Compton scattering off an intense laser [1]. The new horizons opened by these possibilities have only recently started to be explored. But also colliding electron beams can be obtained at no extra cost and moreover with high degrees of polarization. As a matter of fact, e^-e^- collisions are excellent experiments for detecting slight deviations from the expectations of the electroweak sector of the standard model. Indeed, QCD enters the game here only at the two-loop level. Of the many possible uses that springs to one's mind [2, 3, 4, 5], not the least is an examination of the electroweak gauge sector. This would, in principle, be of twofold use: first the verification of the standard model at the one-loop level, and more interestingly, as a search for new physics beyond the electroweak scale.

In a previous study [6] we examined the effect of anomalous $WW\gamma$ and WWZ trilinear gauge couplings on the total cross section of the reaction

$$e^-e^- \rightarrow e^-\nu_e W^- . \quad (1)$$

It was seen that this novel approach gives results that are as good as those obtainable by other methods and, more interestingly, provides a complementary tool. The importance of the latter aspect is easily appreciated as one attempts to unravel the potentially complex structure of this sector of the theory. Here we refine the aforementioned analysis by considering the same reaction with polarized incoming electron beams and by taking into account the angular distribution of the outgoing electron. The use of polarized beams provides two complementary experiments which turn out to explore different regions of the five-dimensional parameter space considered here. The resolving power of the reaction is also significantly enhanced by the study of angular distributions instead of just total cross sections.

We plan the rest of the article as follows. In section 2 we give a brief introduction to the possible anomalous couplings, consistent with certain symmetry properties, that are relevant for the interaction (1). We also indicate the constraints (direct and indirect) that have so far been obtained in the literature. Section 3 examines the standard model expectations for the above process in some detail. This indicates the relevant kinematical cuts that lead to a more efficient extraction of the signal. In section 4 we begin by examining the quantitative effect that the presence of anomalous couplings have on the total cross section. This is followed by a discussion on the angular distributions and the statistical significance of any bounds thus obtained. Section 5 contains our results in the form of contours of detectability for different planes of the five-dimensional parameter space. Our conclusions are then summarized in section 6.

2 Anomalous Couplings

In the standard model, the tree-level self-couplings of the vector bosons are of course dictated by the gauge principle. Deviations from such couplings could arise from two different (but inter-related) sources : (i) quantum corrections and (ii) the presence of a new threshold nearby the weak scale and/or the “gauge bosons” themselves being composite objects. The quantum corrections in the standard model have been investigated [7] and turn out to be rather small. Precisely due to this, any evidence of deviation from the standard couplings would be an unmistakable signature for the existence of a new physics realm, thus delivering us from the pessimistic ‘Big Desert’ scenario.

An obvious arena for detecting such effects would be to look for their effect on precisely measured low-energy processes. Indeed such studies[8] had initially claimed that precision measurements at LEP had already ruled out deviations large enough to be directly measurable in the near future. These analyses were criticised though on two accounts[9]: (i) the use of a $SU(2)_L \otimes U(1)_Y$ gauge dependent Lagrangian; and (ii) an improper use of the cut-off procedure to regulate divergent integrals. A way out of this impasse was pointed out by Burgess and London[10] who showed that any Lorentz and electromagnetic gauge invariant Lagrangian for W 's and Z 's automatically obeys $SU(2)_L \otimes U(1)_Y$ gauge invariance, realized nonlinearly in general. Furthermore, only the logarithmic divergences are relevant for the issues at hand. Subsequent reexaminations, both in the case of a non-linearly realized $SU(2)_L \otimes U(1)_Y$ symmetry with an arbitrary symmetry breaking sector[11], or that of a decoupling theory [12] show that the constraints imposed by LEP data are considerably weaker than claimed previously¹. This methodology however has an inherent “weakness” in that the answers depend crucially on the assumptions made about the higher theory. Such exercises are therefore no substitute for direct measurements.

In our discussion, we shall restrict ourselves only to WWZ and $WW\gamma$ couplings. Analogous studies for quartic boson couplings [13] or for triple neutral boson vertices [14] have been performed by other authors. We shall furthermore restrict the analysis to C and P conserving couplings. Though CP -violating terms in the Lagrangian would contribute to the cross sections that we are interested in, these are best isolated by looking at final state asymmetries[15]. The effective Lagrangian parametrizing the WWV vertex ($V = \gamma, Z$) can then be expressed as[16]

$$\mathcal{L}_{eff}^{WWV} = -ig_V \left[g_V^1 \left(W_{\alpha\beta}^\dagger W^\alpha - W^{\dagger\alpha} W_{\alpha\beta} \right) V^\beta + \kappa_V W_\alpha^\dagger W_\beta V^{\alpha\beta} + \frac{\lambda_V}{M_W^2} W_{\alpha\beta}^\dagger W^\beta V^{\sigma\alpha} \right] \quad (2)$$

where $V_{\alpha\beta} = \partial_\alpha V_\beta - \partial_\beta V_\alpha$ and $W_{\alpha\beta} = \partial_\alpha W_\beta - \partial_\beta W_\alpha$.

In Eq. (2), g_V is the WWV coupling in the standard model *viz.* ,

$$g_\gamma = e, \quad g_Z = e \cot \theta_W \quad (3)$$

where θ_W is the weak mixing angle. Of the other couplings, only g_γ^1 is constrained by electromagnetic gauge invariance to be unity, and the rest are model dependent. In the

¹In fact, if such an analysis were to be naively extended beyond the region of validity of a momentum expansion, the constraints would turn out to be rather weak [11].

standard model we have

$$g_Z^1 = \kappa_\gamma = \kappa_Z = 1 \quad \text{and} \quad \lambda_\gamma = \lambda_Z = 0. \quad (4)$$

It should be noted that the couplings κ_V , λ_V and g_Z^1 are not really constants but actually represent form factors and hence, in principle, are energy-dependent. It can then be seen easily that even higher dimensional operators can essentially be written in terms of these quantities.

Till date, the only direct constraints are those obtained for κ_γ and λ_γ from an analysis of the process $p\bar{p} \rightarrow e\nu\gamma X$ at the Collider Detector at Fermilab (CDF) [17] and at UA2 at CERN [18]. Assuming these events to have arisen from W -decay consequent to $W\gamma$ production, parts of the κ_γ - λ_γ plane could be ruled out [19]. The constraints are still very weak though, especially when compared to the one-loop contributions in the standard model [7].

The above limits can be improved somewhat though at HERA [20], but owing to the relatively low luminosity and energy and also due to large background noise, strong limits on the Z -couplings are not expected. The situation is poised for dramatic improvement both in the context of upcoming machines like LEP-200 and the LHC [21, 22] as well as future linear colliders operating either in the traditional e^+e^- mode [23], or as $e\gamma$ and $\gamma\gamma$ colliders [24].

3 Standard Model Expectations

The Feynman diagrams contributing at lowest order to the scattering process (1) are depicted in Fig. 1. If both electron beams are right-polarized the process does not take place, because at least one of the fermion lines is connected to a W boson. For the LR combination of initial helicities, diagram 4, in which a W is exchanged between the two fermion lines, does not contribute. For the LL configuration, the same diagrams with the initial electrons exchanged have to be added. In all calculations we ignore the electron mass, as is justified at the energies considered.

The diagrams with a virtual photon induce a collinear singularity which is regulated only by the electron mass. Nevertheless, this dangerous region of phase space is naturally avoided by a simple acceptance cut on the angle of the emerging electron with the beam axis. Throughout the rest of this paper we have thus imposed the rapidity cut

$$|\eta(e^-)| < 3 \quad \text{or} \quad |\cos\theta(e^-)| < .995 \quad \text{or} \quad 5.7^\circ < \theta(e^-) < 174.3^\circ. \quad (5)$$

To ensure that the outgoing electron is indeed visible, we also required a minimum energy of 10 GeV:

$$E(e^-) > 10 \text{ GeV}. \quad (6)$$

There are several sources of background to the process (1). Leptonic decays of the W^- cannot be distinguished from non-resonant lepton production $e^-e^- \rightarrow e^-\nu_e\ell^-\nu_\ell$, which

proceeds via the exchange of a virtual W^- and a Z^0 or γ . In order to avoid this irreducible background altogether, we thus concentrate only on the hadronic decays of the W^- . In this case, the competing non-resonant mechanisms can be reduced to an innocuous level by an invariant mass measurement of the jets, the very act of W reconstruction. Still Z^0 Bremsstrahlung $e^-e^- \rightarrow e^-e^-Z^0$ could be mistaken for our signal if one of the outgoing electrons disappears along the beampipe. To avoid this background we have also demanded an imbalance in the observed transverse momentum of the event:

$$p_{\perp}(e^- + W^-) > 10 \text{ GeV} . \quad (7)$$

The dependence of the resulting standard model cross section as a function of the center of mass energy is shown in Fig. 2 for the two combinations of beam polarizations², LL and LR . Clearly, the LL configuration dominates, so that almost all conclusions drawn for it also apply as well for unpolarized beams. Note the wide threshold region, which is typical for vector boson production. The decrease of the cross section at large energies is due to the cut (5).

It is interesting to dwell a little on the expected topology of these events, which is significantly different for each combination of initial polarizations as well as at low and high energy.

3.1 LR Polarization

To facilitate the following discussions, let us label for the time being the two incoming left-handed and right-handed electrons respectively e_L and e_R and the outgoing particles e , W and ν .

At low energy, the dominant diagrams are those which involve a photon exchange, *i.e.* diagrams 2 and 3. Because of the low transverse momentum transfer of the photon, e stays close to the original trajectory of e_R . The rest of the reaction can then be seen as an electron-photon t -channel scattering $e_L\gamma^* \rightarrow \nu W$, where the photon is almost on-shell and aligned with e_R . In the $e_L\gamma^*$ center of mass frame, W strongly tends to emerge opposite to e_L [25]. This trend remains even after boosting back to the laboratory frame, as is shown in Fig. 3a. The observed e and W tend thus to emerge into the detector in the same direction, as can be inferred from Fig. 3b. Note, however, the little bump in the distribution at larger angles, which is due to the Z^0 exchange diagrams.

At high energy, all diagrams contribute with comparable strength. Still e tends to be even less scattered away from the direction of e_R . However, the first diagram of Fig. 1 induces now an important fraction of events where W is emitted in the same direction as the initial e_L , as can be seen in Fig. 3a. The observed e and W can thus now be emitted

²Since very high degrees of longitudinal polarization should be available at future linear colliders, for simplicity we assume 100% polarization in the following. The effects of dilution can be easily incorporated, though.

both parallel as well as anti-parallel. This is shown in Fig. 3b, where the low-energy bump becomes a peak.

The energy of e and especially ν is always strongly peaked close to the beam energy. In contrast, the energy of W is distributed more broadly, with a strong tendency to be emitted at rest, though.

3.2 LL Polarization

The picture is now tainted by the interferences of diagram 4 of Fig. 1 with the three others. At low energies, the angular distributions in Figs 4 can still be explained by the competing trends of diagrams 2, 3 and diagram 4. The latter favours events with W and e back-to-back and transverse to the beam direction. In contrast, diagrams 2 and 3, similarly to the LR case, favour collinear topologies. The resulting e angular distribution is peaked along the beampipe, whereas the W and We angular distributions are rather flat.

At high energies, the interferences become strongly destructive and it stops making sense to talk of the contributions of individual diagrams. The general trend is the same as at low energies, just with a more enhanced peaking.

As for the LR case the energy of e and especially ν is strongly peaked close to the beam energy, whereas the energy of W is distributed more broadly, with a strong tendency to be emitted at rest.

Examples of typical event topologies for both polarization modes are depicted in Fig. 5.

4 Calculations

In the following, we have only considered a center of mass energy of 500 GeV, restricting our study to the case of a typical linear collider of the next generation. In this case the standard model cross section is 3.19 pb for LL beams and 0.348 pb for LR beams.

The dependence of the total cross sections on each of the couplings can be seen from Figs 6. For each of these curves, all the other couplings have been held to their standard model values. As is easily seen, the dependence on the $WW\gamma$ couplings is more pronounced than on the WWZ couplings, irrespective of the beam polarization. This can be traced back to the higher mass of the Z^0 .

Note that while the cross section as a function of the dimension six operators is nearly symmetric about the standard model value of $\lambda_{\gamma,Z} = 0$, this certainly is not the case for the other three. Thus a measurement of the total cross section alone cannot resolve potentially large values of these couplings from the standard model point. This is precisely the reason why the consideration of angular distributions is important. Before we embark on that, note that the dependence of cross section on κ_Z and g_Z^1 is quite different for

the two beam polarizations. This will obviously be important in unravelling the WWZ couplings from the $WW\gamma$ ones.

The standard model differential cross section as a function of the angle of the emerging electron is displayed for both polarization schemes in Fig. 7. The poles in the directions of the beams are never reached, thanks to the angular cut (5). Also shown are the distributions for one particular anomalous value of κ_V each ($\kappa_Z = -2.15$ for LL and $\kappa_\gamma = -1.1$ for LR). Although they differ significantly from the standard model distributions, the total cross section is almost the same in either case. These examples show how important it is to consider angular correlations.

In the following we shall thus subdivide the angular range (5) in 20 bins for the LL case and in 10 bins for the LR case. For a given choice of anomalous gauge parameters we compare the content of each bin with the standard model expectation. Instead of the angle of the emerging electron with the beam axis, one could as well have chosen another variable, such as the angle of the W^- or the ν_e , or the energy or transverse momentum of any combination of the particles. None of these, though, can be measured with as little systematic uncertainties³.

To estimate the resolving power of the reaction (1), we compute the χ^2 function

$$\chi^2 = \sum_{i=1}^{bins} \left| \frac{N_{SM}(i) - N_{anom}(i)}{\Delta N_{SM}(i)} \right|^2, \quad (8)$$

where N_{SM} is the number of events predicted by the standard model and N_{anom} is the number of events effectively measured in the presence of anomalous gauge couplings. The sum runs over all 10 (LR) or 20 (LL) bins in $\theta(e^-)$ over the allowed range (5). The number of events $N = \mathcal{L}\sigma\epsilon_W$ is calculated assuming a typical design integrated luminosity $\mathcal{L} = 10 \text{ fb}^{-1}$ and a branching ratio for hadronic decays of the W^- of $\epsilon_W \approx 2/3$. The error in Eq. (8) is a combination of statistical and systematic errors

$$\Delta N = \sqrt{(\sqrt{N})^2 + (\delta_{syst}N)^2}. \quad (9)$$

Since the emergence angle of an electron should be measurable to an accuracy better than 10 mrad, the main systematic errors originate from the luminosity measurement and from detector efficiencies. Since these should not exceed 1%, we conservatively assume an overall systematic uncertainty of 2% (*i.e.* $\delta_{syst} = .02$). The error is thus dominated by the statistical fluctuations which amount to an average per bin of 2.5% for the LL and 5.5% for the LR beam polarizations.

To avoid spurious results, a bin is rejected from the analysis (*i*) if the difference between the standard model expectation and the measured number of events is less than one and (*ii*) if the standard model expectation is less than one event while the measured number is less than three. In order not to lose significant statistics because of these restrictions, we have used less angular bins for the LR initial polarizations.

³ It turns out that the polar angle of the W^- is actually a more sensitive variable than the polar angle of the e^- . If its resolution can be improved, its use might thus yield even more precise results.

5 Results

We present our results in terms of the χ^2 function (8), for different combinations of two anomalous gauge couplings:

$$(\kappa_\gamma, \kappa_Z) \quad (\lambda_\gamma, \lambda_Z) \quad (\kappa_\gamma, \lambda_\gamma) \quad (\kappa_Z, \lambda_Z) \quad (\kappa_Z, g_Z^1)$$

For each of these combinations the other three parameters are kept to their standard model value. The corresponding $\chi^2 = 2, 4, 6$ contours are displayed in Figs 8-12. Their probabilistic interpretation is the following⁴: The areas of the parameter space lying outside each contour can be explored with 63.2%, 86.5% and 95% confidence respectively. If only one of the parameters is of interest, irrespective of the values taken by the other, the half-planes beyond the edges of the three contours can be explored with 84.3%, 95.4% and 98.6% confidence respectively. If one of the parameters is known to take its standard model value, the latter confidence levels are valid for the half-lines bounded by the intersections of the contours with the axis.

Taken individually, the *LL* and *LR* combinations of initial helicities show a strong correlation of the $\kappa_{\gamma,Z}$ and $\lambda_{\gamma,Z}$ parameters⁵. Fortunately, the combined *LL* and *LR* data almost entirely lifts this correlation and provides much tighter bounds on the parameters. The same phenomenon also takes place in the (κ_Z, λ_Z) and (κ_Z, g_Z^1) planes, to a lesser extent, though. In spite of its lower overall cross section, the *LR* beam polarization generally yields tighter bounds on the parameters. This can be traced back to the absence of the W^- exchange diagram, which otherwise dominates but is not sensitive to anomalous couplings. A reduction of the systematical error would greatly improve the *LL* results.

A comparison of the resolving power at 90% confidence level ($\chi^2 = 2.71$) of different experiments is given in Table 1. Here we only consider one anomalous coupling at a time, all others being assumed to take their standard model value. Although this assumption is not realistic, it allows at least a simple comparison and may help to provide guidelines⁶.

It appears that HERA, LEP2 and TEVATRON are unlikely to provide competitive results. In contrast, the high energies obtained at LHC make it the best tool for studying higher dimensional operators, *i.e.* the λ parameters. None of the four possible operation modes of a linear collider of the next generation seems to dominate the others. Note, however, that the $e^- \gamma$ and $\gamma \gamma$ modes do not probe the Z^0 sector. This can be seen as a disadvantage if considered individually, but certainly constitutes a major advantage when the information gathered from each experiment is combined. Indeed, it is important to remember that, if at all, most likely several or all anomalous gauge parameters would assume non-trivial

⁴ It has to be taken with a grain of salt, though, since the problem is not linear and the errors are not necessarily gaussian. This becomes particularly clear in Figs 10-12.

⁵ As matter of fact, if the electronic angular distribution is not taken into account, this correlation assumes a dramatic form for the κ parameters [6]: a large closed band of values of the parameters cannot be distinguished from the standard model case.

⁶Note that the strong upper limit on κ_Z obtained in ref.[22] is not from direct observability, but rather deduced from radiative correction bounds. Also the authors postulate relations between the various couplings.

values. It might, therefore, be dangerous to discard one particular experiment as being insensitive, only on the basis of the comparison in Table 1.

6 Conclusion

We have demonstrated that e^-e^- scattering provides a useful reaction to investigate the gauge sector of the standard model. Indeed, slight modifications of the trilinear $WW\gamma$ and WWZ gauge couplings would show up as measurable deviations from the standard model expectations of the outgoing electron's angular distribution in the process $e^-e^- \rightarrow e^-\nu_e W^-$. A straightforward χ^2 analysis on data obtained at a typical linear collider of the next generation, would reveal or exclude values of the five C and P conserving anomalous gauge coupling parameters, which are competitive with those obtained in e^+e^- , $e^-\gamma$ and $\gamma\gamma$ collisions.

In view of the large number of parameters at hand and their possibly interfering effects, many experiments would be needed to disentangle their individual contributions. In this respect, e^-e^- collisions already offer the bonus that the two possible beam polarizations yielding the required signal, probe complementary regions of the parameter space.

Nevertheless, even in the presence of an unmistakable departure from the standard model prediction in a given experiment, it is important to remember that it is only the conjunction of as many experiments as possible which might provide the means to understand the origin of this anomaly. This is why linear colliders, which can be operated in e^+e^- , e^-e^- , $e^-\gamma$ and $\gamma\gamma$ modes, will be privileged tools for the study of anomalous gauge couplings.

We are very much indebted to Edward Boos and Michael Dubinin for having provided us with the CompHEP software [26], which we have used to generate some of the matrix elements used in this study.

References

- [1] I.F. Ginzburg, G.L. Kotkin, V.G. Serbo and V.I. Telnov, *Nucl. Instr. Meth.* **205** (1983) 47.
- [2] P.H. Frampton and D. Ng, *Phys. Rev. D* **45** (1992) 4240.
- [3] F. Cuypers, G.J. van Oldenborgh and R. Rückl, *Nucl. Phys. B* **409** (1992) 128.
- [4] C.A. Heusch and P. Minkowski, CERN preprint CERN-TH-6606-92, May 1993.
- [5] D. Choudhury, F. Cuypers and A. Leike, MPI preprint MPI-PhT/94-23, April 1993.
- [6] D. Choudhury and F. Cuypers, *Phys. Lett. B* (in press).
- [7] G. Couture *et al.*, *Phys. Rev. D* **36**, 859 (1987).
- [8] A. de Rujula, M.B. Gavela, P. Hernandez and E. Masso, *Nucl. Phys.* **B384**, 3 (1992); J.J. van der Bij, *Phys. Lett.* **B296**, 239 (1992). See also other papers cited in Ref.[10].
- [9] M.B. Einhorn and J. Wudka, ITP, Santa Barbara Report NSF-ITP-92-01 (1992)(unpublished); Michigan U. Report UM-TH-92-25(unpublished); J. Wudka, University of California Report UCRHEP-108 (1993) (unpublished).
- [10] C.P. Burgess and D. London, *Phys. Rev. Lett.* **69**, 3428 (1992), C.P. Burgess and D. London, *Phys. Rev.* **D48**, 4337 (1993).
- [11] D. Choudhury, P. Roy, and R. Sinha, TIFR preprint TIFR-TH/93-08 (1993).
- [12] K. Hagiwara *et al.* , *Phys. Lett.* **B283**, 353 (1992); *Phys. Rev.* **D48**, 2182 (1993); D. Zeppenfeld and R. Szalapski, *Proc. Warsaw Symp.* (1992); D. Zeppenfeld *et al.* , *Proc. DPF Conf.* (1992); P. Hernández and F.J. Vegas, *Phys. Lett.* **B307**, 116 (1993).
- [13] G. Bélanger and F. Boudjema, , *Proc. Munich, Annecy, Hamburg Workshop, e^+e^- Collisions at 500 GeV, February 4 to September 3, 1991*, ed. P.M. Zerwas.
- [14] H. Czyz *et al.* , *Phys. Scripta* **41**, 197 (1990); D. Choudhury and S.D. Rindani, MPI preprint MPI-PhT/94-21, April 1993.
- [15] H.S. Mani, B. Mukhopadhyaya and S. Raychaudhuri, M.R.I, Allahabad preprint MRI-PHY/9/93 (1993); D. Chang *et al.* , CERN preprint, CERN-TH.6839/93 (1993).

- [16] K. Hagiwara, R.D. Peccei and D. Zeppenfeld, *Nucl. Phys.* **B282**, 253 (1987); J.F. Gaemers and G.J. Gounaris, *Z. Phys.* **C1**, 259 (1979).
- [17] M. Timko, ‘Status of $W\gamma$ Search at CDF’, contribution to *The Spring Meeting of the American Physics Society*, Washington, D.C., 16-19 April 1990 (unpublished).
- [18] J. Alitti *et al.*, *Phys. Lett.* **277B**, 194 (1992).
- [19] M. Samuel, G. Li, N. Sinha, R. Sinha and M.K. Sundaresan, *Phys. Lett.* **B280**, 124 (1992).
- [20] W.H. Smith *et al.*, *Proc. Summer Study on High Energy Physics in the 1990s, Snowmass, 1988*, ed. S. Jensen (World Scientific).
- [21] M.Davier *et al.*, in *Proc. of the “ECFA Workshop on LEP 200”*, Eds A. Böhm and W. Hoogland (1987), CERN 87-08.
- [22] G.L. Kane, J. Vidal and C.P. Yuan, *Phys. Rev.* **D39**, 2617 (1989).
- [23] P. Kalyniak *et al.*, *Phys. Rev.* **D48**, 5081 (1993); A.A. Likhoded *et al.*, ICTP preprint IC/93/288 (1993).
- [24] S.Y. Choi and F. Schrempp, *Phys. Lett.* **B272**, 149 (1991); E. Yehudai, *Phys. Rev.* **D44**, 3434 (1991).
- [25] F. Cuypers, G.J. van Oldenborgh and R. Rückl, *Nucl. Phys.* **B 383** (1992) 45.
- [26] E. Boos *et al.*, in: *New Computing Techniques in Physics Research*, eds. D. Perret-Gallix and W. Wojcik, Paris, 1990, p. 573.

machine or experiment	g_Z^1		κ_γ		κ_Z		λ_γ		λ_Z	
	min	max	min	max	min	max	min	max	min	max
UA2 [18, 19]			-3.1	4.2			-3.6	3.5		
TEVATRON [19]			-2.4	3.7						
HERA [20]			0.5	1.5			-2	2		
TEVATRON [22]			0.5	1.8	0.2		-0.2	0.2	-0.4	0.4
LHC [22]			0.8	1.2	0.8		-0.02	0.02	-0.03	0.03
LEP2 [22]			0.86	1.87	0.76		-0.4	0.4	-0.4	0.4
LC500 e^+e^- [24]			0.985	1.14			-0.02	0.04		
LC500 $e\gamma$ [24]			0.96	1.04			-0.05	0.05		
LC500 $\gamma\gamma$ [24]			0.98	1.015			-0.04	0.075		
LC500 e^-e^-	0.91	1.07	0.985	1.015	0.96	1.04	-0.045	0.075	-0.11	0.06

Table 1: Parameter values which can be tested by a particular experiment at 90% C.L. The boldfaced numbers correspond to limits already set. For the generic 500 GeV linear collider LC500, we have assume an integrated luminosity of 10 fb^{-1} for electron or photon beams. For the e^-e^- option we have used the combined information from LL and LR beam polarizations.

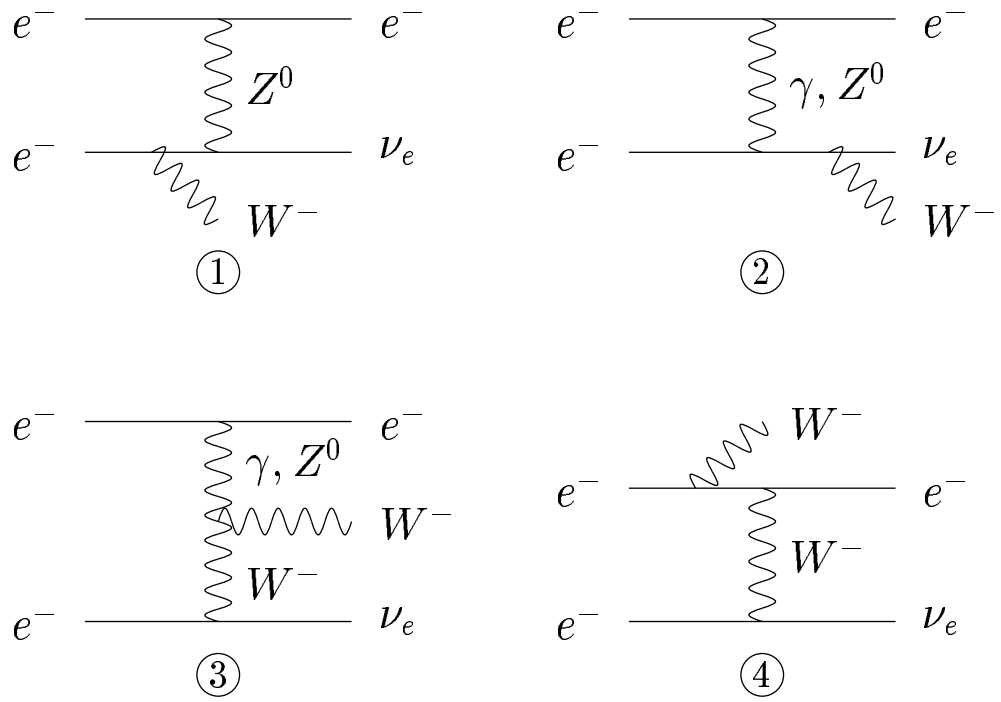


Figure 1: Lowest order Feynman diagrams contributing to the process (1).

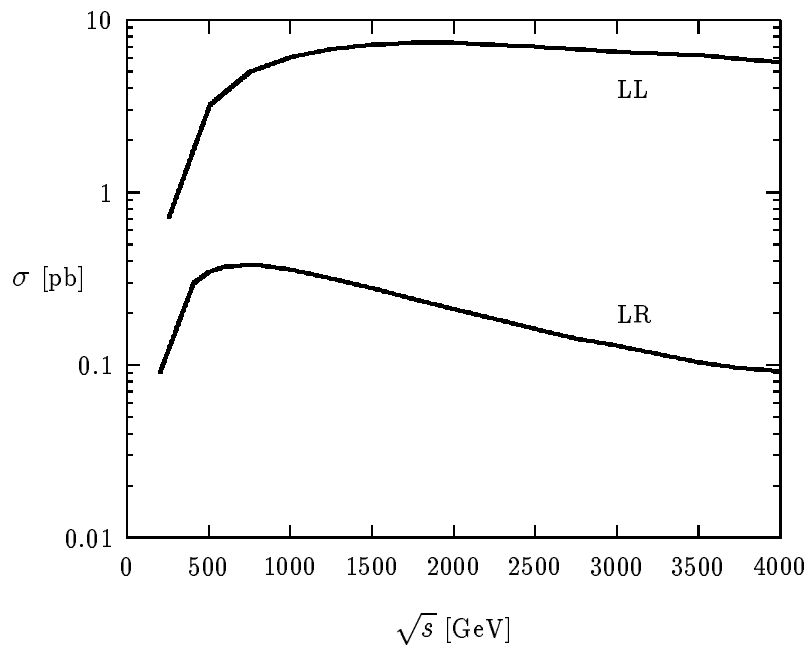


Figure 2: Standard model cross sections of the process (1) as a function of the center of mass energy for both possible combinations of beam polarizations.

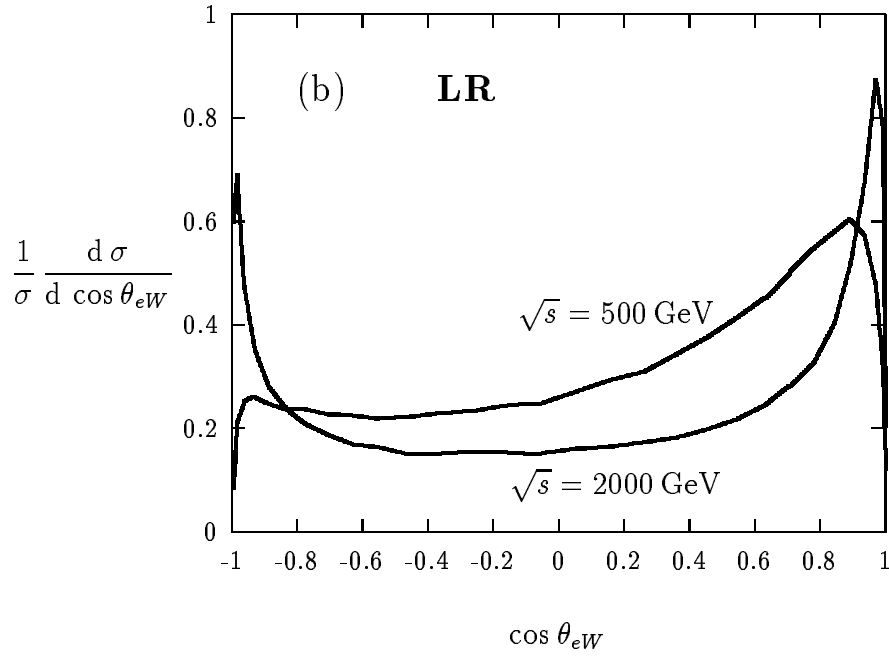
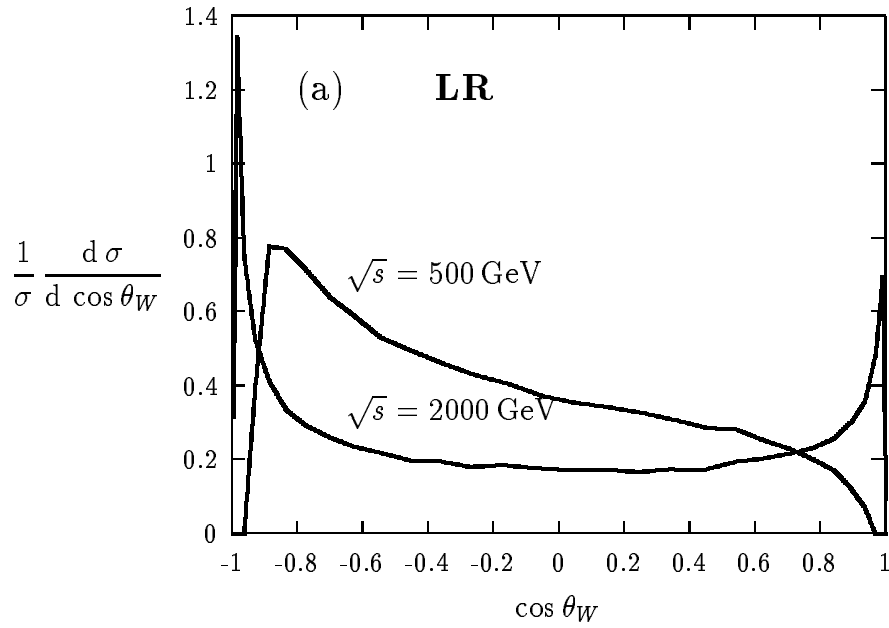


Figure 3: Standard model low and high energy distributions of (a) the angle of the W^- with respect to the left-polarized beam, (b) the angle spanning the emerging W^- and e^- . One of the beams is left-, the other right-polarized.

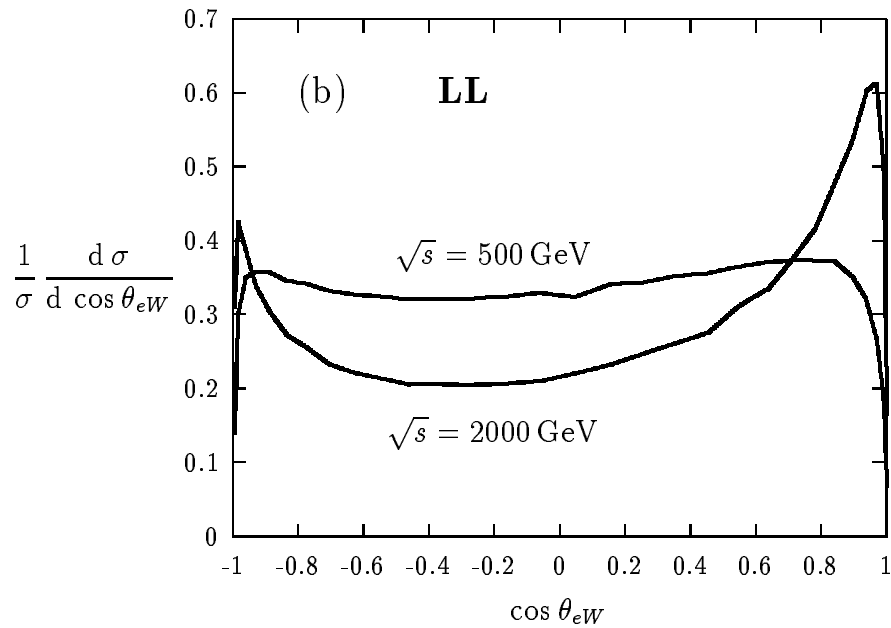
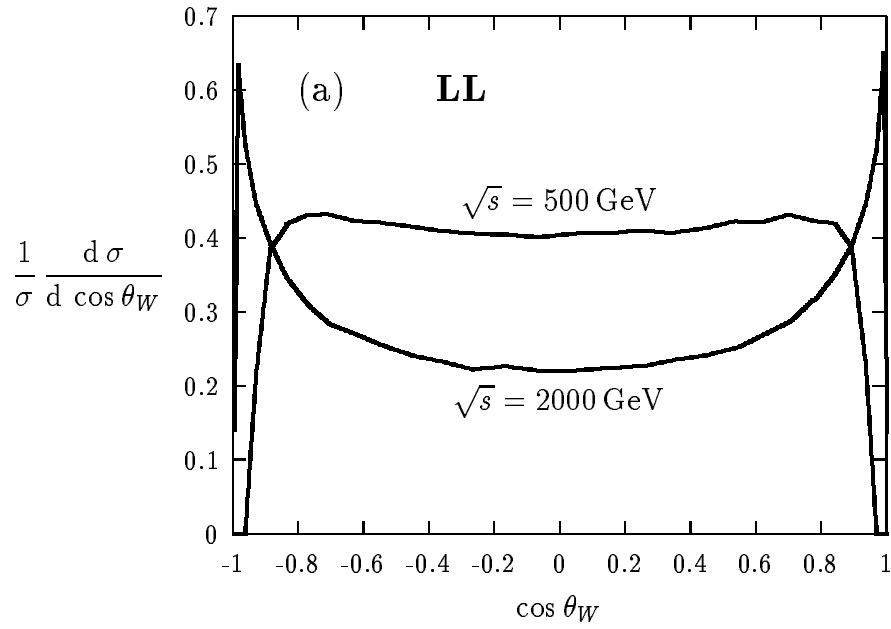


Figure 4: Same as Fig. 3, for both beams being left-polarized.

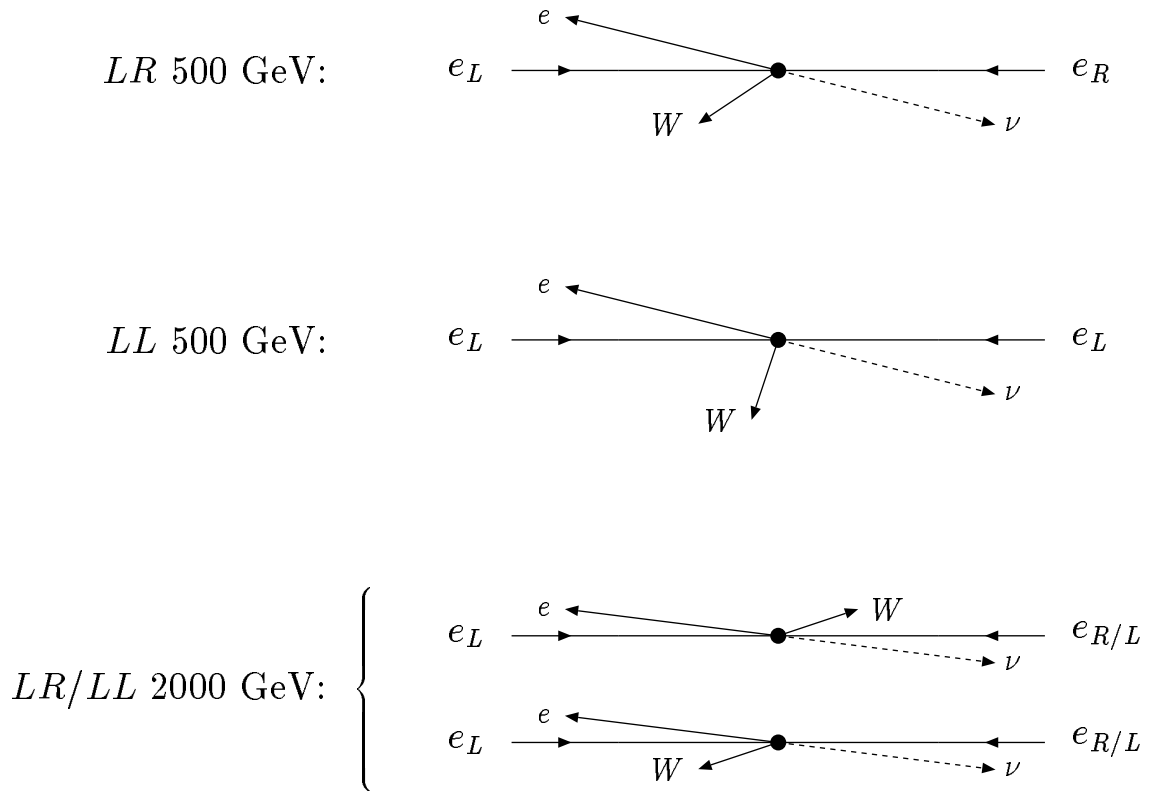


Figure 5: Typical event topologies. The arrows represent the three-momenta of the particles.

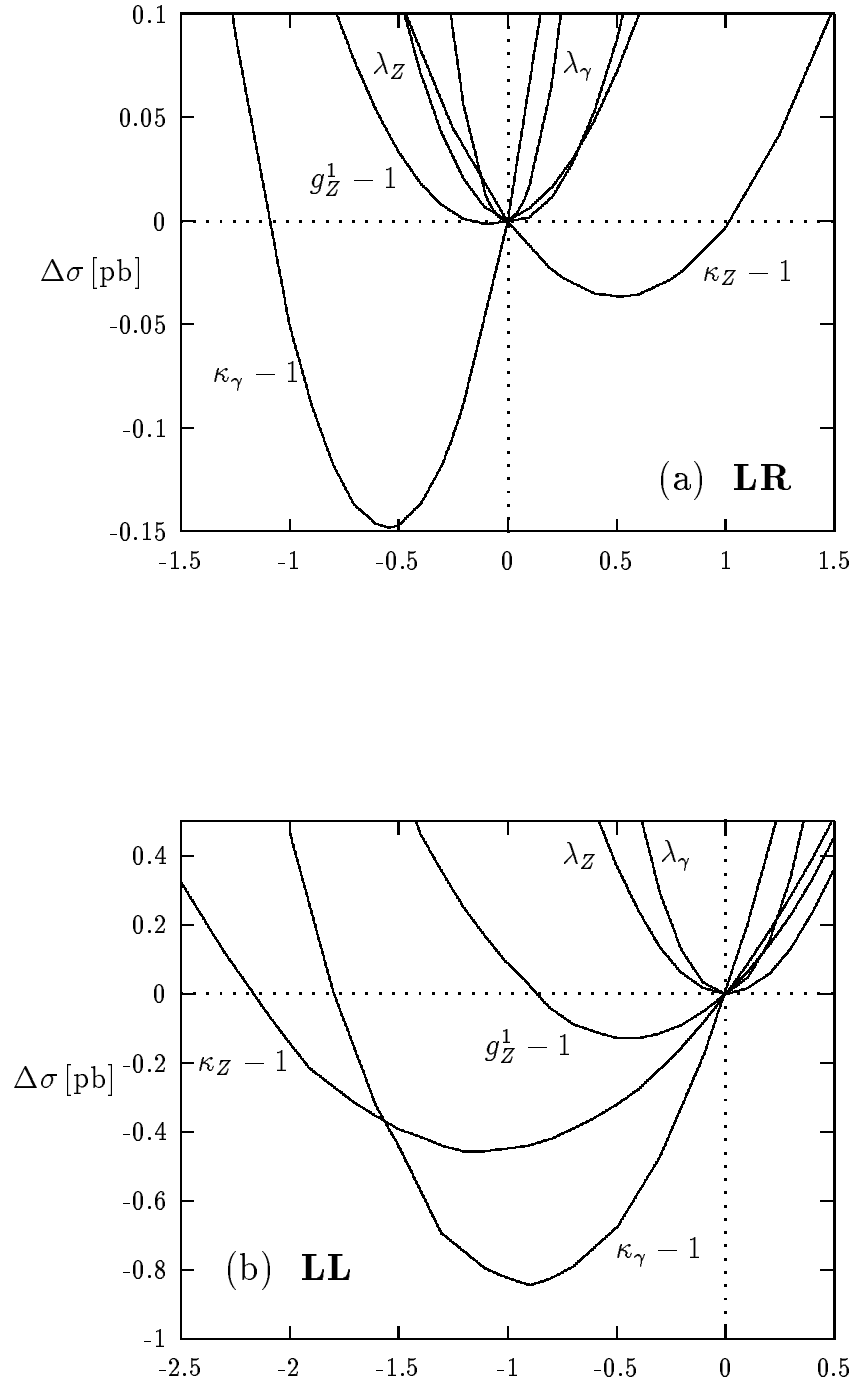


Figure 6: Contribution to the total cross section of each of the anomalous couplings, while all others are held to their standard model values. The standard model cross sections are 3.19 pb for *LL* polarization and 0.348 pb for *LR*.

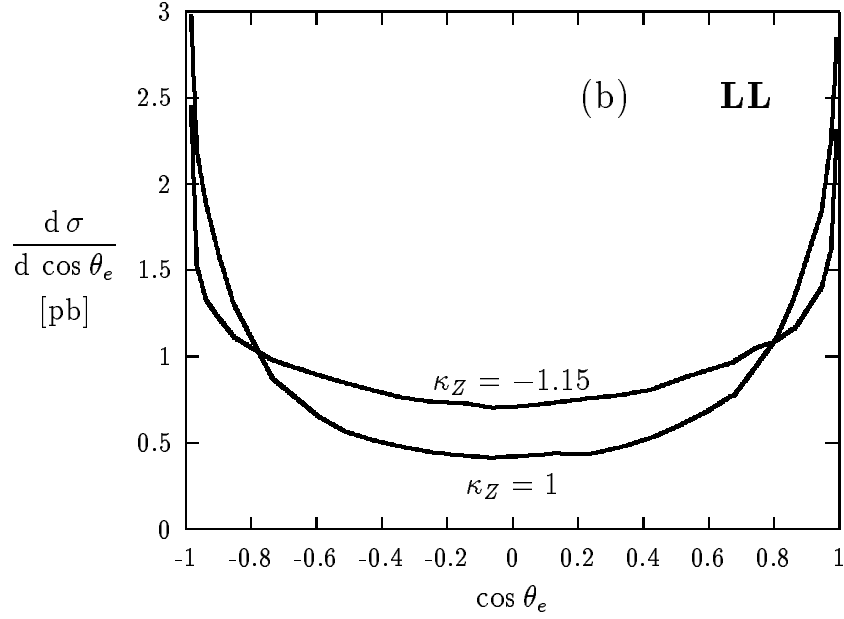
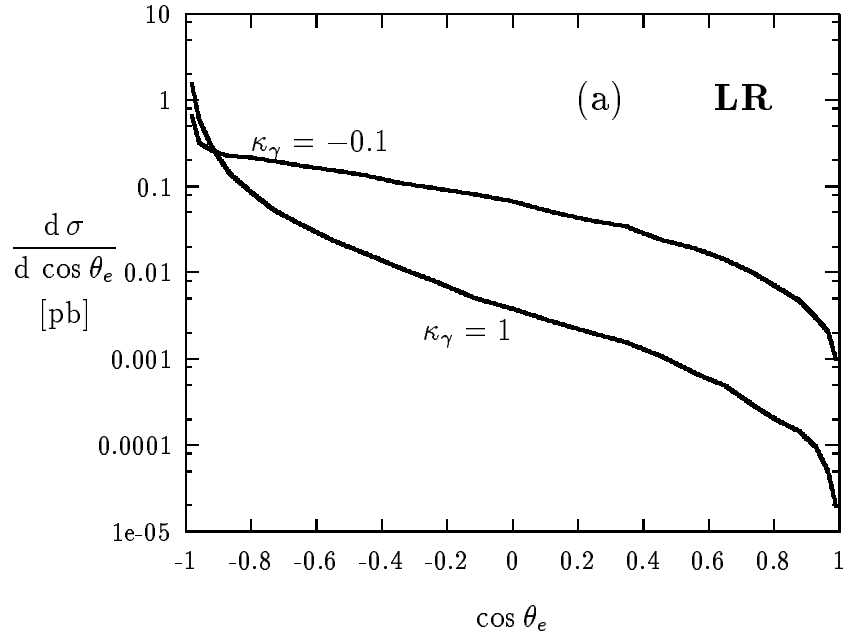


Figure 7: Differential distributions for particular values of the anomalous couplings which lead to the same integrated cross section as the one expected from the standard model.

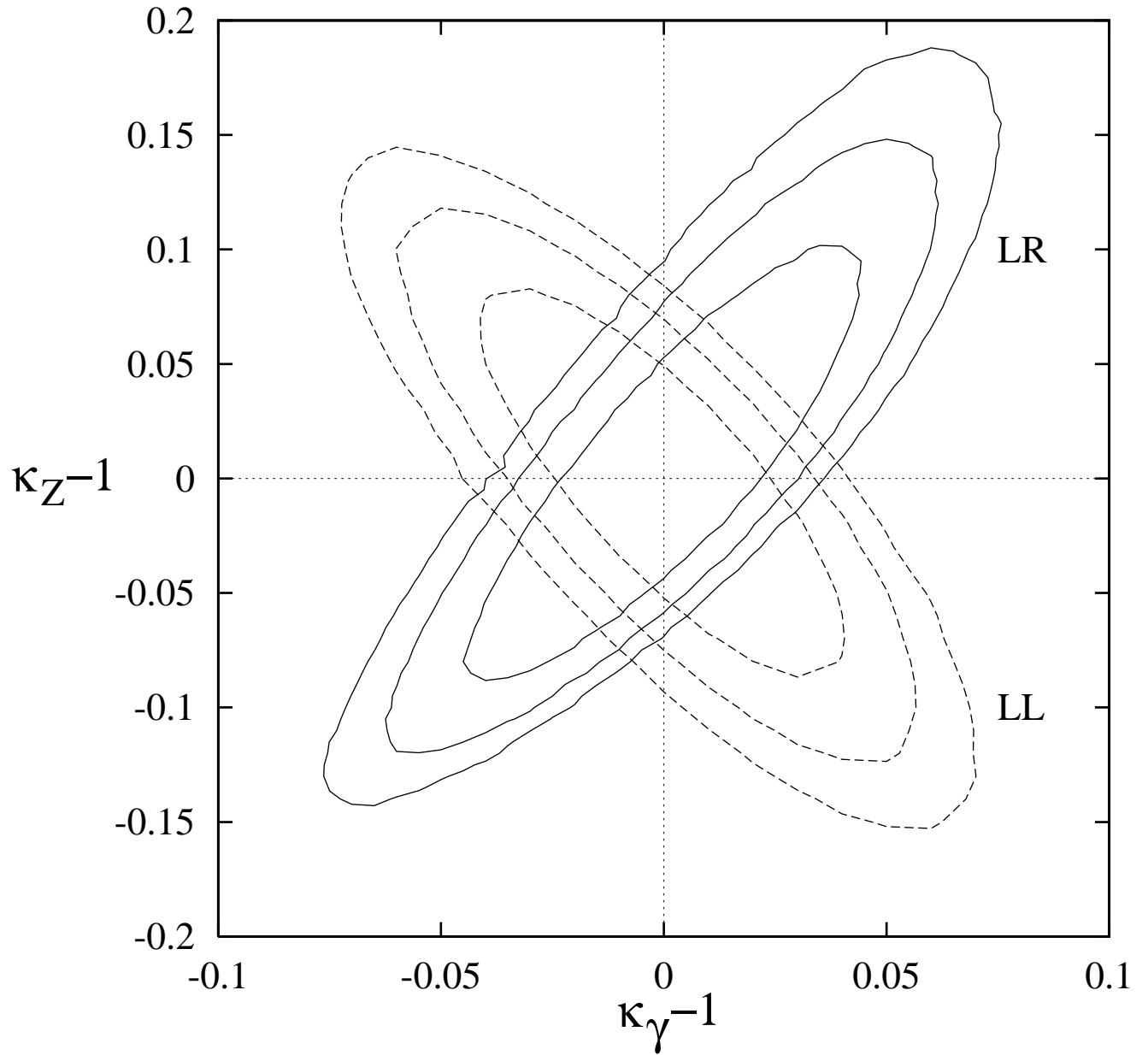


Figure 8: Contours of detectability at different confidence levels ($\chi^2 = 2, 4, 6$ — see Eq. (8)) in the $\kappa_\gamma - \kappa_Z$ plane for *LL* (dashed lines) and *LR* (solid lines) polarizations. The remaining couplings assume their standard model values.

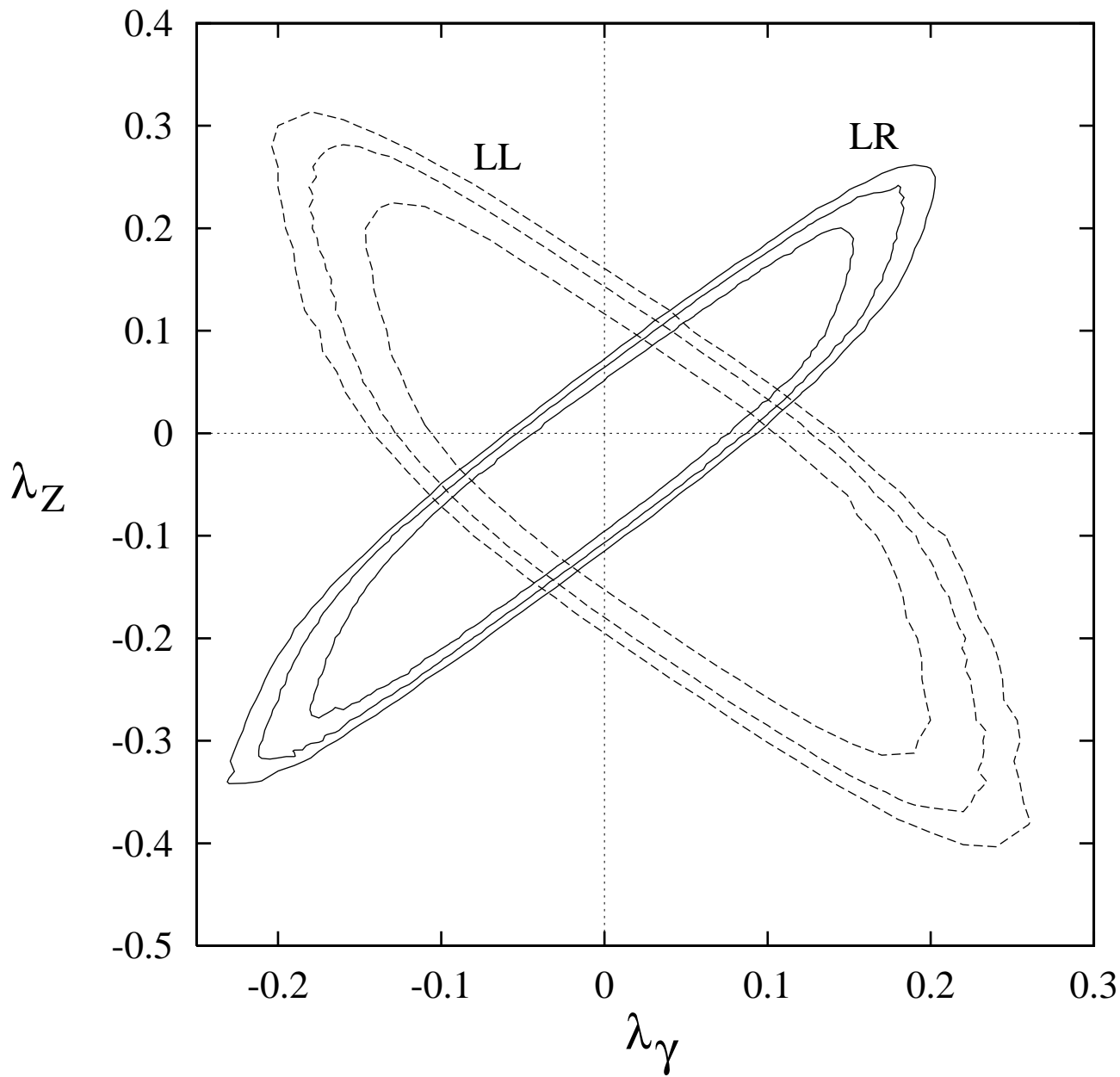


Figure 9: As in Fig. 8, but in the λ_γ - λ_Z plane instead.

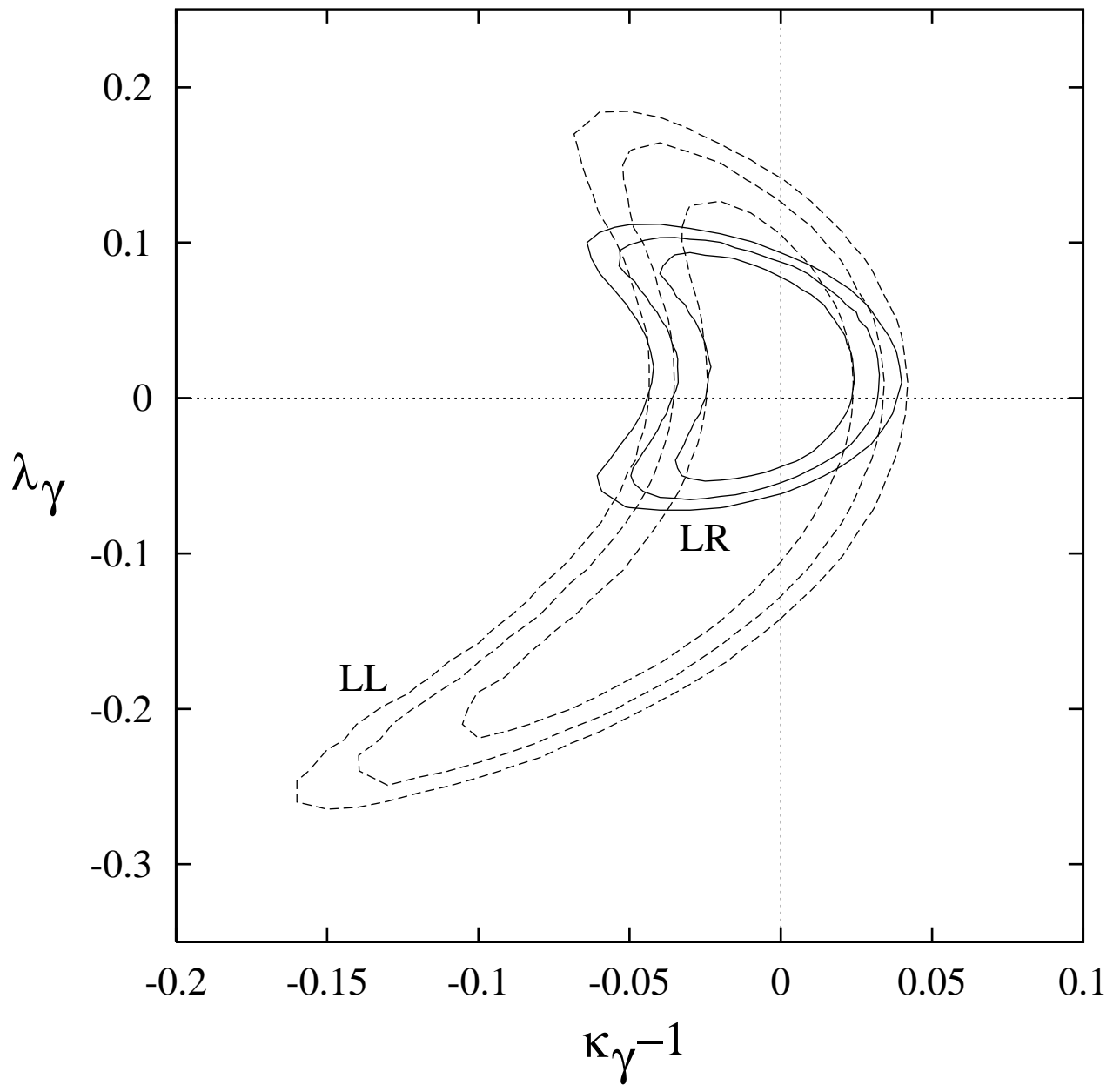


Figure 10: As in Fig. 8, but in the $\kappa_\gamma - \lambda_\gamma$ plane instead.

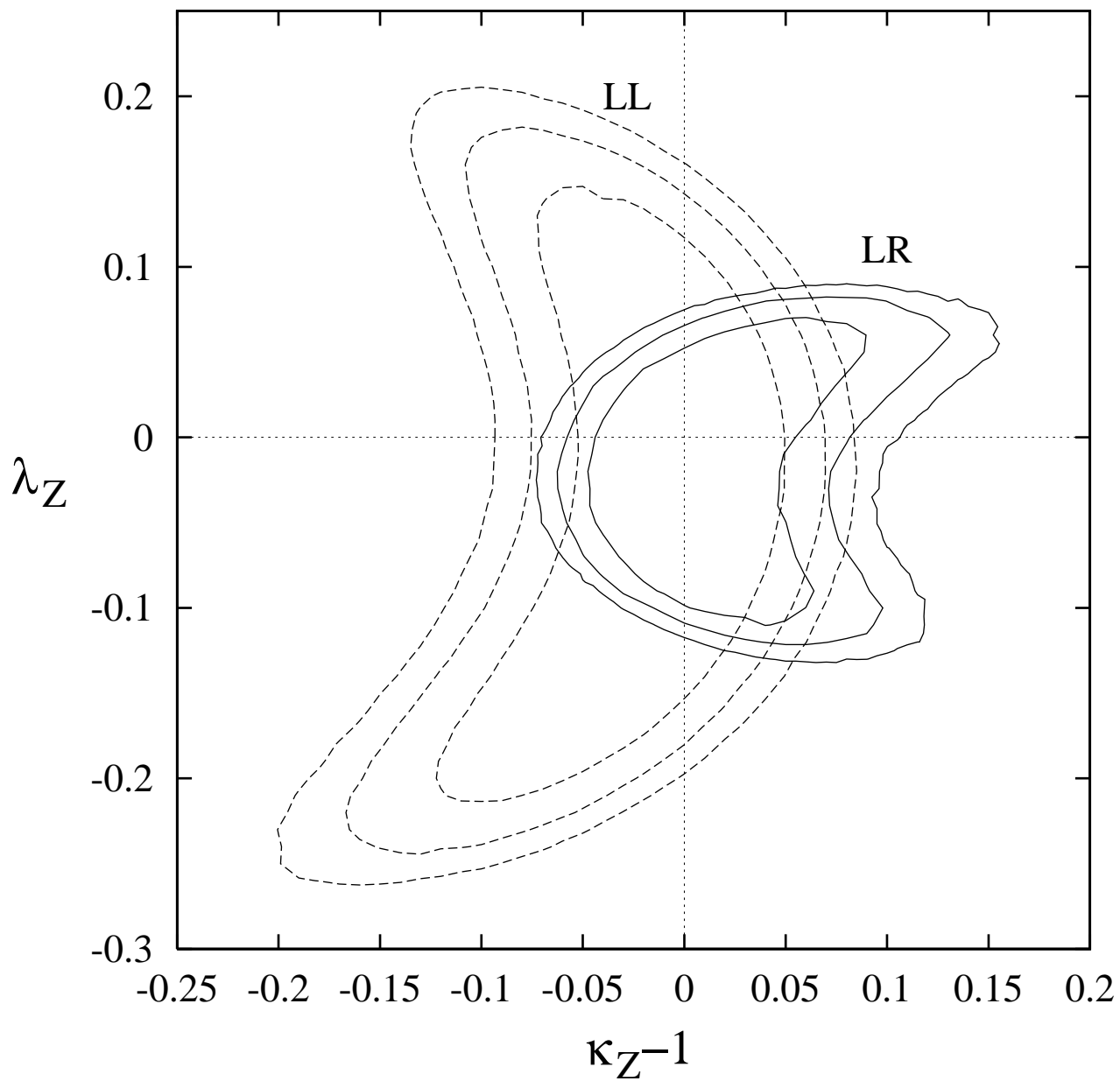


Figure 11: As in Fig. 8, but in the $\kappa_Z - \lambda_Z$ plane instead.

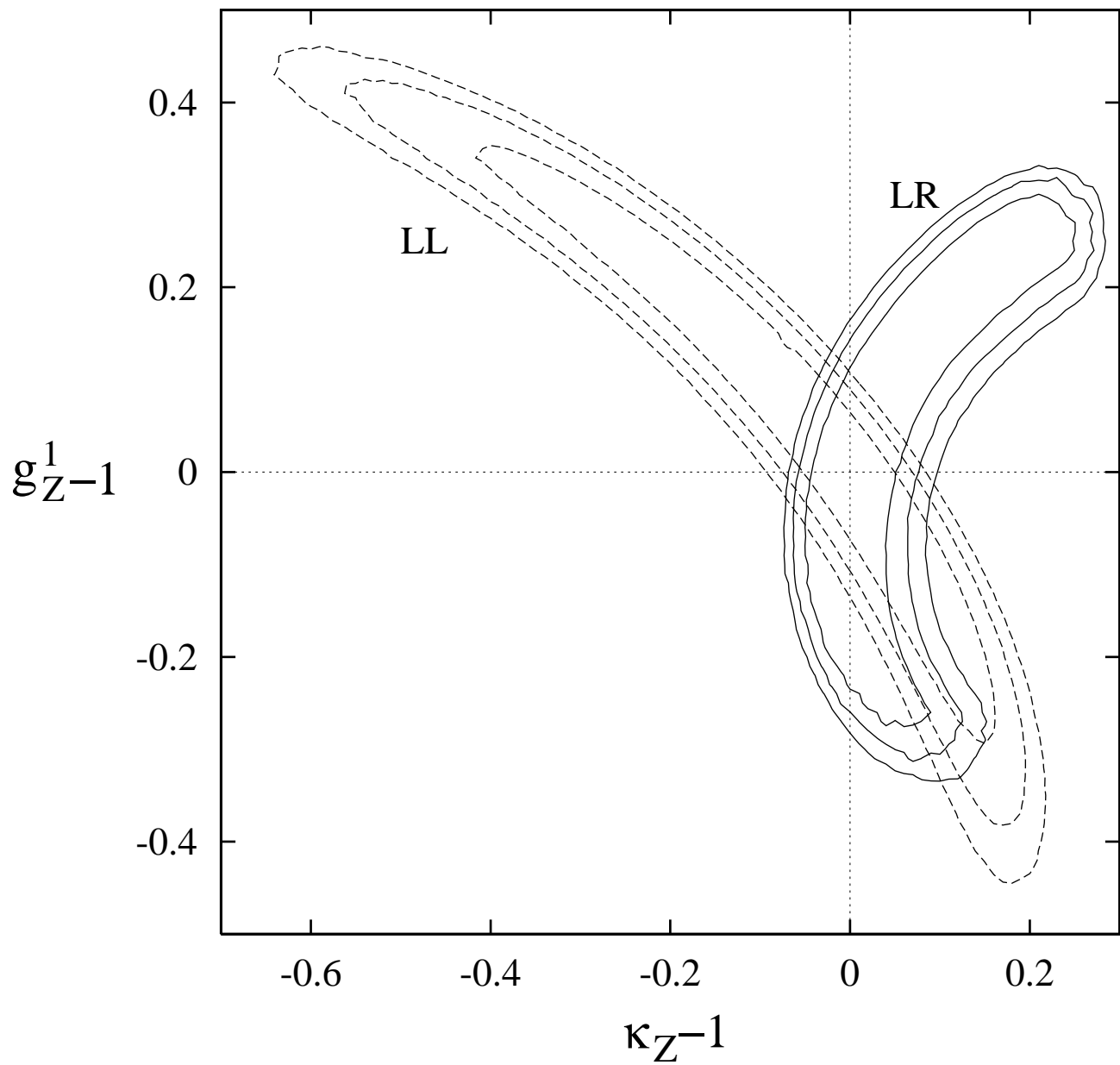


Figure 12: As in Fig. 8, but in the $\kappa_Z - g_Z^1$ plane instead.